Article

Heats of Formation of Co(CO)NOPR, R = CH and CH$_2$, and Its Ionic Fragments

Zsolt Gengeliczki, Blint Sztray, Tomas Baer, Christopher Iceman, and Peter B. Armentrout

J. Am. Chem. Soc., **2005**, 127 (26), 9393-9402• DOI: 10.1021/ja0504744 • Publication Date (Web): 14 June 2005

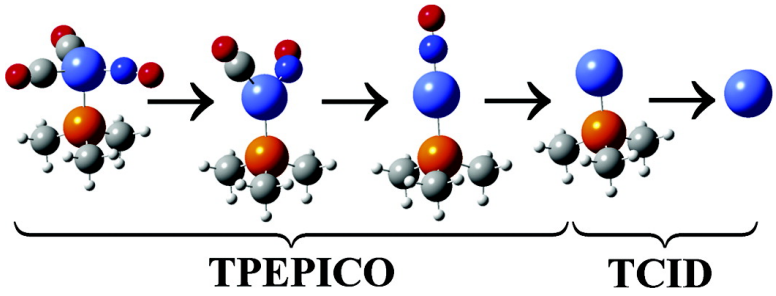

J|A|C|S
ARTICLES
Published on Web 06/14/2005

Heats of Formation of $Co(CO)_2NOPR_3$, R = CH_3 and C_2H_5, and Its Ionic Fragments

Zsolt Gengeliczki,[†] Bálint Sztáray,*[,†] Tomas Baer,[‡] Christopher Iceman,[§] and Peter B. Armentrout[§]

Contribution from the Department of General and Inorganic Chemistry, Eötvös Loránd University, Budapest, Hungary, Department of Chemistry, University of North Carolina, Chapel Hill, North Carolina 27599-3290, and Department of Chemistry, University of Utah, Salt Lake City, Utah 84112-0850

Received January 24, 2005; E-mail: szb@elte.hu

Abstract: A joint threshold photoelectron photoion coincidence spectrometry (TPEPICO) and collision-induced dissociation (CID) study on the thermochemistry of $Co(CO)_2NOPR_3$, R = CH_3 (Me) and C_2H_5 (Et), complexes is presented. Adiabatic ionization energies of 7.36 ± 0.04 and 7.24 ± 0.04 eV, respectively, were extracted from scans of the total ion and threshold electron signals. In the TPEPICO study, the following 0 K onsets were determined for the various fragment ions: $CoCONOPMe_3^+$, 8.30 ± 0.05 eV; $CoNOPMe_3^+$, 9.11 ± 0.05 eV; $CoPMe_3^+$ 10.80 ± 0.05 eV; $CoCONOPEt_3^+$, 8.14 ± 0.05 eV; $CoNOPEt_3^+$, 8.92 ± 0.05 eV; and $CoPEt_3^+$, 10.66 ± 0.05 eV. These onsets were combined with the Co^+-PR_3 (R = CH_3 and C_2H_5) bond dissociation energies of 2.88 ± 0.11 and 3.51 ± 0.17 eV, obtained from the TCID experiments, to derive the heats of formation of the neutral and ionic species. Thus, the $Co(CO)_2NOPR_3$ (R = CH_3 and C_2H_5) 0 K heats of formation were found to be −350 ± 13 and −376 ± 18 kJ·mol^{-1}, respectively. These heats of formation were combined with the published heat of formation of $Co(CO)_3NO$ to determine the substitution enthalpies of the carbonyl to phosphine substitution reactions. Room-temperature values of the heats of formation are also given using the calculated harmonic vibrational frequencies. Analysis of the TCID experimental results provides indirectly the adiabatic ionization energies of the free phosphine ligands, $P(CH_3)_3$ and $P(C_2H_5)_3$, of 7.83 ± 0.03 and 7.50 ± 0.03 eV, respectively.

Introduction

Transition metal complexes are used as catalysts in numerous reactions important in biology and industry. Their effectiveness depends on several factors of which the availability of metal sites that can participate in the chemical reaction is of paramount importance. An especially interesting group of complexes is the transition metal carbonyls. In these compounds, the usual starting step for the formation of the catalytically active, coordinatively unsaturated species is metal−carbonyl bond rupture. Therefore, the thermochemistry, especially the transition metal−carbonyl bond energies, is vitally important. In the past few years, our groups have studied the neutral and ionic gas-phase thermochemistry of a number of organometallic complexes, such as $CpCo(CO)_2$,[1,2] $CpMn(CO)_3$,[3] $BzCr(CO)_3$,[4] Cp_2Mn,[5] Bz_2Cr,[6] and $Co(CO)_3NO$[7] (Cp = C_5H_5, Bz = C_6H_6) as well as the unsaturated homoleptic metal carbonyls of Ti^+,[8] V^+,[9] Cr^+,[10] Fe^+,[11] Co^+,[12] Ni^+,[13] Cu^+,[14] Ag^+,[14] and Pt^+.[15]

Cobalt tricarbonyl nitrosyl has an important role in synthetic organic chemistry,[16−18] chemical vapor deposition,[19−21] and even nanotechnology.[22,23] On the other hand, experiments show that phosphine substitution may strongly affect the stability and catalytic activity of transition metal carbonyls.[24−26] Both steric effects[27] and electronic factors related to the phosphines are

[†] Eötvös Loránd University.
[‡] University of North Carolina.
[§] University of Utah.

(1) Sztáray B.; Baer, T. *J. Am. Chem. Soc.* **2000**, *122*, 9219.
(2) Sztáray B.; Szepes L.; Baer, T. *J. Phys. Chem. A* **2003** *107*, 9486.
(3) Li, Y.; Sztáray, B.; Baer, T. *J. Am. Chem. Soc.* **2001**, *123*, 9388.
(4) Li, Y.; Sztáray, B.; Baer, T. *J. Am. Chem. Soc.* **2002**, *124*, 4487.
(5) Li, Y.; Sztáray, B.; Baer, T. *J. Am. Chem. Soc.* **2002**, *124*, 5843.
(6) Li, Y.; Sztáray, B. *J. Phys Chem.* **2002**, *106*, 9820.
(7) Sztáray, B.; Baer, T. *J. Phys. Chem. A* **2002**, *106*, 8046.
(8) Meyer, F.; Armentrout, P. B. *Mol. Phys.* **1996**, *88*, 187.
(9) Sievers, M. R.; Armentrout, P. B. *J. Phys. Chem.* **1995**, *99*, 8135−8141.
(10) Khan, F. A.; Clemmer, D. E.; Schultz, R. H.; Armentrout, P. B. *J. Phys. Chem.* **1993**, *97*, 7978.
(11) Schultz, R. H.; Crellin, K. C.; Armentrout, P. B. *J. Am. Chem. Soc.* **1991**, *113*, 8590.
(12) Goebel, S.; Haynes, C. L.; Khan, F. A.; Armentrout, P. B. *J. Am. Chem. Soc.* **1995**, *117*, 6994.
(13) Khan, F. A.; Steele, D. L.; Armentrout, P. B. *J. Phys. Chem.* **1995**, *99*, 7819.
(14) Meyer, F.; Chen, Y.-M.; Armentrout, P. B. *J. Am. Chem. Soc.* **1995**, *117*, 4071.
(15) Zhang, X.-G.; Armentrout, P. B. *Organometallics* **2001**, *20*, 4266.
(16) Pályi, Gy.; Sampár Szerencsés, E.; Galamb, V.; Palágyi, J.; Markó, L. Hungarian patent HU 87-2105, 19870511, 1989.
(17) Roustan, J. L.; Bisnaire, M.; Park, G.; Guillaume, P. *J. Organomet. Chem.* **1988**, *356*, 195.
(18) Kubota, T.; Okamoto, H.; Okamoto, Y. *Jpn. Catal. Lett.* **2000**, *67*, 171.
(19) Lene, P. A.; Oliver, P. E.; Wright, P. J.; Reeves, C. L.; Piit, A. D:û.; Cockayne, B. *Chem. Vap. Deposition* **1998**, *4*, 183.
(20) Ivanova, A. R.; Nuesca, G.; Chen, X.; Goldberg, C.; Kaloyeros, A. E.; Arkles, B.; Sullivan, J. J. *J. Electrochem. Soc.* **1999**, *146*, 2139.
(21) Smart, C. J.; Reynolds, S. K.; Stanis, C. L.; Patil, A.; Kirleis, J. T. *Mater. Res. Soc. Symp. Proc.* **1993**, *282*, 229.
(22) Rana, R. K.; Koltypin, Y.; Gedanken, A. *Chem. Phys. Lett.* **2001**, *344*, 256.
(23) Liu, S.; Zhu, J.; Mastai, Y.; Felner, L.; Gedanken, A. *Chem. Mater.* **2000**, *12*, 2205.
(24) Slaugh, L. H.; Mullineaux, R. D. *J. Organomet. Chem.* **1968**, *13*, 469.

important in this regard. The $Co(CO)_2NOPR_3$, R = CH_3 (Me), C_2H_5 (Et), C_4H_9 (Bu), and C_6H_5 (Ph) complexes seem to be ideal systems to study the influence of tertiary phosphines on the thermochemistry of $Co(CO)_xNO^+$ species. These phosphine derivatives have potentially useful industrial applications, for example, they have been used in metal oxide vapor deposition (MOVD) experiments[28] to obtain clean Co films and they were applied as starting materials in the synthesis of ylide complexes of cobalt.[29]

The thermochemistry and gas-phase ion energetics data for these phosphine complexes and their fragments are poorly characterized. For the case of $Co(CO)_2NOPEt_3$, the first ionization energy (IE) is known from the study of Distefano et al.[30] as 7.62 eV. Recently, HeI photoelectron spectra and vertical ionization energies of $Co(CO)_2NOPR_3$ (R = Me, Et) have been reported.[31]

Multiple values for the IEs of the trimethyl- and triethylphosphine ligands are available in the literature,[32−39] but most of these values are vertical IEs. Studies by Beauchamp and co-workers list adiabatic IEs for PMe_3 as 8.01 ± 0.07 and 8.11 ± 0.10 eV.[36,37] No explanation of the change in the reported IE of the PMe_3 was given. To estimate the adiabatic IE of PEt_3, we note that Wada and Kiser obtained a relative difference in vertical IEs between the trimethyl- and triethylphosphine complexes of 0.33 eV,[32] Yarbrough and Hall obtained 0.27 eV,[39] and Weiner and Lattman list values giving a difference of 0.29 eV.[38] If we combine the average difference of 0.30 ± 0.05 eV with the weighted average of the adiabatic IEs for PMe_3 determined by Beauchamp and co-workers, 8.05 ± 0.10 eV, we estimate an adiabatic IE of 7.74 ± 0.11 eV for PEt_3. This estimate can be compared with an adiabatic IE of 7.61 eV for PEt_3, determined from equilibrium gas-phase measurements by Aue and Bowers.[40]

In the present work, the ionic gas-phase thermochemistry of $Co(CO)_2NOPMe_3$ and $Co(CO)_2NOPEt_3$ has been investigated to systematically examine changes in R. We investigate the gas-phase dissociation kinetics of energy-selected $Co(CO)_2NOPR_3^+$ ions using threshold photoelectron photoion coincidence (TPEPICO) spectroscopy and the dissociation of $CoPR_3^+$ ions using threshold collision-induced dissociation (TCID). The experimental results, interpreted with a statistical analysis of the dissociation rates and the energy partitioning in the dissociation steps, provide bond energies and heats of formation of both neutral $Co(CO)_2NOPR_3$ and its various fragment ions. Combining the heats of formation of the neutral molecules with the known heat of formation of $Co(CO)_3NO$[7] permits the determination of the enthalpy for the following reactions: $Co(CO)_3NO + PR_3 \rightarrow Co(CO)_2NOPR_3 + CO$.

Experimental Section

Preparation of the Samples. The Thorsteinson−Basolo synthesis[41] was used to prepare $Co(CO)_2NOPR_3$ (R = CH_3, C_2H_5). $Co(CO)_3NO$ (8.02 g, 50.0 mmol) was added to 50.0 mL of a room-temperature 1.0 M tetrahydrofurane solution of the appropriate phosphine (50.0 mmol) under an atmosphere of nitrogen. The reaction mixture was stirred for 6 h before the solvent and excess reactants were removed at reduced pressure. In both cases, the product was isolated as a dark red liquid with a yield of >80% and was stored under inert atmosphere at −25 °C until the TPEPICO measurements. $Co(CO)_3NO$ was purchased from Strem Chemicals and was used without further purification. Phosphines were purchased from Sigma-Aldrich in the form of 1.0 M tetrahydrofuran solution.

Threshold Photoelectron Photoion Coincidence Spectroscopy. The details of the TPEPICO spectrometer have been described previously.[42] Because of the sufficiently high vapor pressure of the samples, they were introduced through a room-temperature needle to the ionization region of the spectrometer. The sample was ionized with vacuum ultraviolet (VUV) light from a H_2 discharge lamp dispersed by a 1-m normal incidence vacuum monochromator. The VUV wavelengths were calibrated using the hydrogen Lyman-α resonance line. The ions and the electrons were extracted in opposite directions with an electric field of 20 V/cm. The electrons were accelerated to about 60 V into the velocity focusing flight tube[43] of 13-cm length. Electrons with zero velocity perpendicular to the extraction voltage were focused to an aperture located in the center of the flight tube, whereas the energetic electrons were focused onto rings around this central spot with radii proportional to their initial velocity perpendicular to the extraction axis. The electrons in the center were detected by a Channeltron electron detector, whereas the electrons with a certain perpendicular velocity were detected by a Chevron stack of multichannel plates with a center hole for the above-mentioned Channeltron. Assuming that the hot electron signal in a ring around the central spot was proportional to the hot electron contribution in the central spot, a weighted fraction of the outer ring signal could be subtracted from the central electrode signal. This procedure corrects the threshold electron signal for the contribution of hot electrons.[44]

The ions were accelerated through 5 cm of the 20 V/cm region, then further accelerated to 220 V before entering a 30-cm-long drift region. They were detected with a multichannel plate (MCP) detector. The electron and ion signals served as start and stop pulses for measuring the ion time-of-flight (TOF), and the TOF for each coincidence event was stored on a multichannel pulse height analyzer. Because both the center and the ring electron signals served as start signals, two TOF distributions were obtained at each photon energy. TOF distributions were obtained in 2−48 h depending on the signal intensity and the desired spectrum quality.

The PEPICO spectra were used for two purposes. First, the fractional abundances of the parent and the daughter ions were measured as a function of the photon energy (breakdown curve). Second, ion decay rates were extracted from asymmetric TOF distributions of the daughter ion signal. This asymmetry is the result of slowly dissociating (metastable) ions dissociating in the 5-cm acceleration region, resulting in a TOF between the parent and the daughter ion's flight time. These

(25) Osborn, J. A.; Jardine, F. H.; Young, G. W. *J. Chem. Soc. A* **1966**, *12*, 1711.
(26) Crabtree, R. *Acc. Chem. Res.* **1979**, *12*, 331.
(27) Tolman, C. A. *J. Am. Chem. Soc.* **1970**, *92*, 2953.
(28) Dickson, R. S.; Yin, P.; Ke, M.; Johnson, J.; Deacon, G. B. *Polyhedron* **1996**, *15*, 2237.
(29) Malisch, W.; Blau, H.; Weickert, P.; Griessmann, K. *Z. Naturforsch., B: Anorg. Chem., Org. Chem.* **1983**, *38B*, 711
(30) Distefano, G.; Innorta, G.; Pignataro, S.; Foffani, A. *J. Organomet. Chem.* **1968**, *14*, 165.
(31) Gengeliczki, Z.; Bodi, A.; Sztaray, B. *J. Phys. Chem. A.* **2004**, *108*, 9957.
(32) Wada, Y.; Kiser, R. W. *J. Phys. Chem.* **1964**, *68*, 2290.
(33) Fischler, J.; Halman, M. *J. Chem. Soc.* **1964**, *1*, 31.
(34) Lappert, M. F.; Pedley, J. B.; Wilkins, B. T.; Stelzer, O.; Unger, E. *J. Chem. Soc., Dalton Trans. 2* **1975**, 1207.
(35) Ostoja Starzewski, K. A.; Bock, H. *J. Am. Chem. Soc.* **1976**, *98*, 8486.
(36) Staley, R. H.; Beauchamp, J. L. *J. Am. Chem. Soc.* **1974**, *96*, 6252.
(37) Hodges, R. V.; Houle, F. A.; Beauchamp, J. L.; Montag, R. A.; Verkade, J. G. *J. Am. Chem. Soc.* **1980**, *102*, 932.
(38) Weiner, M. A.; Lattman, M. *Inorg. Chem.* **1978**, *17*, 1084.
(39) Yarbrough, L. W., II; Hall, M. B. *Inorg. Chem.* **1978**, *17*, 2269.
(40) Aue, D. H.; Bowers, M. T. Stabilities of positive ions from equilibrium gas-phase basicity measurements. In *Gas Phase Ion Chemistry*; Bowers, M. T., Ed.; Academic: New York, 1979; Chapter 9.
(41) Thorsteinson, E. M.; Basolo, F. *J. Am. Chem. Soc.* **1966**, *88*, 3930.
(42) Baer, T.; Booze, J. A.; Weitzel, K. M. Photoelectron Photoion Coincidence Studies of Ion Dissociation Dynamics. In *Vacuum Ultraviolet Photoionization and Photodissociation of Molecules and Clusters*; Ng, C. Y., Ed.; World Scientific: Singapore, 1991; p 259.
(43) Baer, T.; Li, Y. *Int. J. Mass. Spectrom.* **2002**, *219*, 381.
(44) Sztáray, B.; Baer, T. *Rev. Sci. Instrum.* **2003**, *74*, 3763.

two types of information were used together in the data analysis as described in detail below.

Guided Ion Beam Tandem Mass Spectrometer. Details of the guided ion beam tandem mass spectrometer used for TCID studies have been provided elsewhere.[11,45] In brief, cobalt monocations are produced in a DC discharge/flow tube ion source in which a 5-cm-long × 0.64-cm-diameter cobalt rod at approximately 1500 V is sputtered by argon ions formed in the resultant DC/glow discharge. The gas flow is typically composed of 10% argon in helium at flow rates of 6500−9500 sccm, which will maintain a flow tube pressure of approximately 1 Torr. The phosphine ligands are then introduced half a meter downstream and attached to the Co^+ ions by three-body association reactions. The flow conditions used in this ion source provide approximately 10^5 collisions between the ions and the flow gases, which thermalize the ions to room temperature, both rotationally and vibrationally. Thus, ions are assumed to be in their ground electronic states and well described by a Maxwell−Boltzmann distribution at 300 K. Previous work has shown these assumptions to be valid in most cases.[10,11,46−49] After the ions are extracted from the ion source, they are focused and accelerated through a magnetic sector where the complex of interest is mass selected, decelerated to a desired kinetic energy, and finally focused into an octopole ion beam guide. By using radio frequency (rf) fields, the octopole traps ions in the radial direction, while not perturbing the axial velocity because of the steep potential walls that characterize the octopole's trapping well.[50,51] The octopole passes through a reaction gas cell with an effective length of approximately 8 cm that was filled with Xe. Xenon is used as a collision partner because its large polarizability allows for efficient translational energy transfer with the ion complex.[48,52] The instrumental configuration ensures that reactant and product ions are collected efficiently, focused into a quadrupole mass filter for separation, and counted with a Daly-type detector.[53] Ion intensities are then converted to cross sections as detailed previously.[45] Absolute cross section magnitudes are estimated to be accurate within ±20%, and relative cross sections are accurate to ±5%.

Energies in the laboratory (lab) frame of reference are converted to the center-of-mass (CM) frame by the equation $E_{CM} = E_{lab}M/(M + m)$, where M is the mass of Xe and m is the mass of the ion. All the energies listed for the CID experiments are in the CM frame unless otherwise noted. The absolute energy scale and kinetic energy distribution of the ion beam are determined by using the octopole as a retarding energy analyzer as described previously.[45] This procedure limits uncertainties from any contact potentials, space charge effects, or focusing aberrations when determining the energy zero and the energy distribution, where the full width half-maximum (fwhm) of the latter is typically 0.2−0.4 eV (lab).

Previous experiments[11,48,54] have shown that the CID cross sections are affected by multiple collisions with the neutral collision partner even when gas cell pressures of the neutral are kept low. For this reason, the pressure dependence of all experiments is explicitly measured because it is difficult to predict when multiple collisions will have an effect on cross section shapes. For these experiments, Xe pressures used were around 0.06, 0.12, and 0.25 mTorr and pressure extrapolations to zero were performed. In all cases, the cross section data shown below have been extrapolated to zero pressure to provide accurate single collision cross sections.

Experimental Results

TPEPICO Studies of $Co(CO)_2NOPMe_3$ and $Co(CO)_2NOPEt_3$. Scans of the total ion and threshold electron signals were used to extract the adiabatic ionization energies of 7.36 ± 0.04 and 7.24 ± 0.04 eV for $Co(CO)_2NOPMe_3$ and $Co(CO)_2NOPEt_3$, respectively. (As usual, our IE value of the trimethylphosphine complex is lower than the value determined by electron impact ionization (EI) in the literature.[30] This is probably because of the unfavorable EI threshold law, which makes it difficult to determine a precise ionization energy.) TOF mass spectra of both compounds were collected in the photon energy range from 8.0 to 13.5 eV. Typical TOF distributions with hot electrons subtracted are shown in Figure 1a−f. The top three spectra are for $Co(CO)_2NOPMe_3$, and the bottom three spectra are for the ethyl analogue. The experimental data are plotted as dots, whereas the solid lines show the fitted TOF distributions as discussed in the data analysis section. Three sequential dissociation reactions associated with the loss of CO, CO, and NO are observed for both compounds upon photoionization between 8 and 13.5 eV (reactions 1−3).

$$Co(CO)_2NOPR_3^+ \rightarrow CoCONOPR_3^+ + CO \quad (1)$$

$$CoCONOPR_3^+ \rightarrow CoNOPR_3^+ + CO \quad (2)$$

$$CoNOPR_3^+ \rightarrow CoPR_3^+ + NO \quad (3)$$

The spectra at low photon energies, shown in Figure 1a,d, correspond to the loss of the first CO group. At higher energies, in spectra of Figure 1b,e, the CO loss fragment ion becomes the parent ion for the next CO loss reaction. Finally, at still higher energies, $CoNOPR_3^+$ ion loses the NO ligand (Figure 1c,f).

At the lowest energies for each fragmentation reaction, the fragment ion TOF distributions are asymmetric, which indicates that the reaction is slow and takes place while the ions are accelerating in the first acceleration region. The fittings of these asymmetric TOF distributions using Rice−Ramsperger−Kassel−Marcus (RRKM) calculated rate constants discussed below are shown as solid lines.

Figure 2, parts a and b, shows the breakdown diagram of the dissociation of $Co(CO)_2NOPR_3^+$ (R = Me and Et, respectively). The fractional abundances of the molecular ion and the fragment ions are plotted as a function of the photon energy. The points are the experimentally determined ratios after the hot electron subtraction, whereas the solid lines show the results of the RRKM simulations, briefly outlined below. Interesting features of the breakdown diagrams are the slopes of the breakdown curves at the crossover points. In the case of the first dissociation, $Co(CO)_2NOPR_3^+ \rightarrow CoCONOPR_3^+ + CO$, the breakdown of the parent ion abundance is quite steep, indicating a narrow distribution of the ion internal energy. The second and the third crossovers, corresponding to the carbonyl loss from $CoCONOPR_3^+$ and to the nitrosyl loss from $CoNOPR_3^+$, are increasingly wider, indicating wider distributions of ion internal energies.

(45) Ervin, K. M.; Armentrout, P. B. *J. Chem. Phys.* **1985**, *83*, 166.
(46) Dalleska, N. F.; Honma, K.; Armentrout, P. B. *J. Am. Chem. Soc.* **1993**, *115*, 12125.
(47) Fisher, E. R.; Kickel, B. L.; Armentrout, P. B. *J. Phys. Chem.* **1993**, *97*, 10204.
(48) Dalleska, N. F.; Honma, K.; Sunderlin, L. S.; Armentrout, P. B. *J. Am. Chem. Soc.* **1994**, *116*, 3519.
(49) Rodgers, M. T.; Armentrout, P. B. *J. Phys. Chem. A* **1997**, *101*, 1238.
(50) Teloy, E.; Gerlich, D. *Chem. Phys.* **1974**, *4*, 417.
(51) Gerlich, D. *Adv. Chem. Phys.* **1992**, *82*, 1.
(52) Aristov, N.; Armentrout, P. B. *J. Phys. Chem.* **1986**, *90*, 5135.
(53) Daly, N. R. *Rev. Sci. Instrum.* **1960**, *31*, 264.
(54) Hales, D. A.; Lian, L.; Armentrout, P. B. *Int. J. Mass Spectrom. Ion Processes* **1990**, *102*, 269.

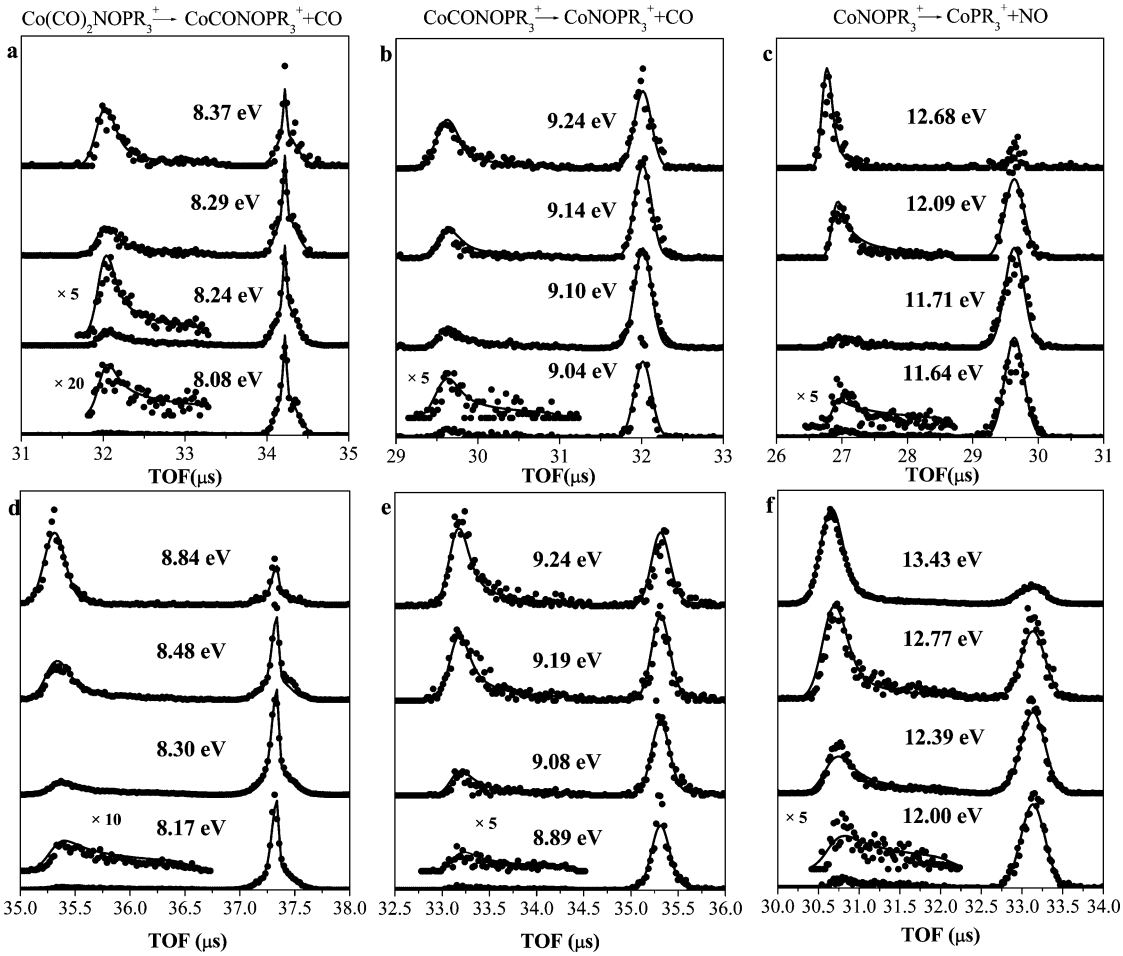

Figure 1. Ion TOF distributions at selected photon energies. Points are the experimental data, whereas the solid lines show the calculated TOF distributions as described in the data analysis. (a−c) Carbonyl and nitrosyl losses from $Co(CO)_2NOPMe_3^+$. (d−f) Dissociation of $Co(CO)_2NOPEt_3^+$ and its fragment ions.

Collision-Induced Dissociation Studies of $CoPMe_3^+$ and $CoPEt_3^+$. Collision-induced dissociation of cobalt trimethylphosphine cations, $CoPMe_3^+$, with Xe was studied over a range of collision energies from 0 to approximately 10 eV. The results, shown in Figure 3, exhibit reactions 4−7.

$$CoPMe_3^+ + Xe \rightarrow CoPH_2Me^+ + C_2H_4 + Xe \quad (4)$$

$$\rightarrow Co^+ + PMe_3 + Xe \quad (5)$$

$$\rightarrow Co + PMe_3^+ + Xe \quad (6)$$

$$\rightarrow Co + PMe_2^+ + Me + Xe \quad (7)$$

The dominant reaction through much of the energy region examined is the CID process 5 in which the metal ion carries the charge. Rising from an apparent threshold approximately 1 eV higher is the alternate charge state reaction 6, in which the phosphine ligand carries the charge. At higher energies, the PMe_3^+ product ion can undergo further dissociation by losing a methyl group, reaction 7. The lowest energy channel is reaction 4, in which ethene is eliminated to form a stable phosphine ligand, PH_2Me, still attached to the cobalt ion. Clearly this process is a much more complicated reaction than the simple bond cleavages. Competition among these various channels explains why the cross section for the kinetically disfavored reaction 4 declines at higher energies. It is interesting that the dissociation of the uncomplexed PMe_3^+ ion leads only to H, CH_3, and CH_4 loss, but not ethylene loss.[55] Evidently, the presence of the cobalt catalyzes the latter rearrangement reaction.

CID of cobalt triethylphosphine cation with Xe yields three sequences of products as shown in Figure 4. At low energies, ethene is lost in reaction 8, yielding a stable phosphine ligand, $PHEt_2$ attached to Co^+. At higher energies, additional ethene molecules are lost sequentially in reactions 9 and 10. Another sequence starts at higher energies and involves loss of the neutral cobalt atom, reaction 11. The primary PEt_3^+ product ion undergoes subsequent loss of ethene molecules in reactions 12 and 13. Competing with the $PEt_3^+ + Co$ (reaction 11) is its charge-transfer partner, $Co^+ + PEt_3$ (reaction 14) in which the cobalt retains the charge. However, in contrast to the trimethylphosphine reaction, the lower energy channel now produces PEt_3^+. Consequently, the Co^+ channel has a much smaller absolute cross section in the $CoPEt_3^+$ reaction than it does in the $CoPMe_3^+$ reaction. These contrasting results are clearly influenced by the relative ionization energies of the

(55) Bodi, A.; Kercher, J. P.; Baer, T.; Sztáray, B. *J. Phys. Chem B* **2005**, *107*, 8393.

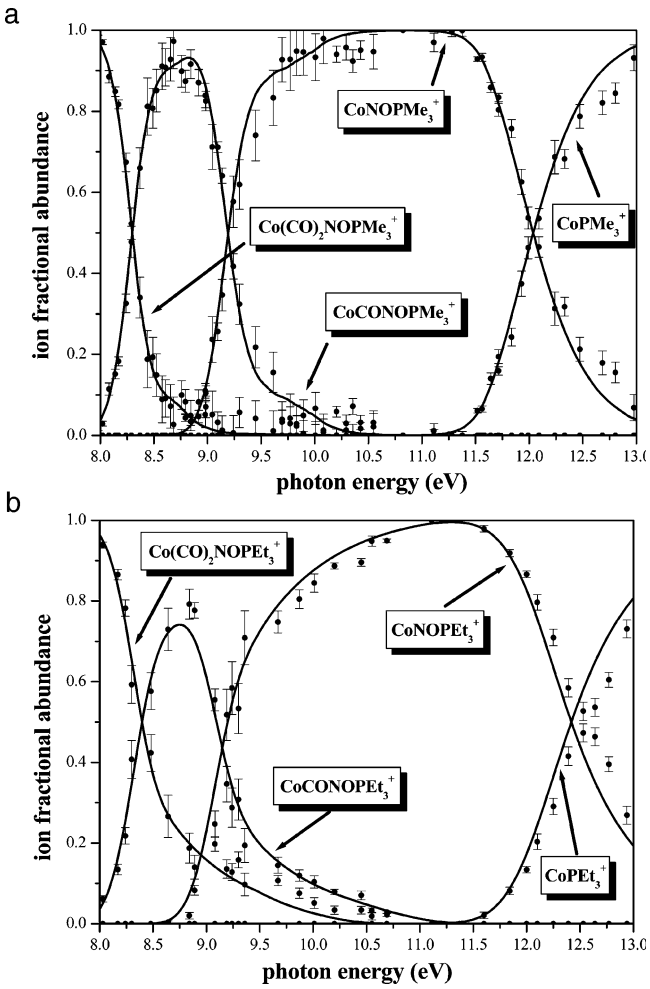

Figure 2. Breakdown curves for the loss of two carbonyl and nitrosyl ligands from (a) $Co(CO)_2NOPMe_3^+$ and (b) $Co(CO)_2NOPEt_3^+$.

phosphine complexes and cobalt atoms, as discussed in more detail below.

$$CoPEt_3^+ + Xe \rightarrow CoPHEt_2^+ + C_2H_4 + Xe \quad (8)$$

$$\rightarrow CoPH_2Et^+ + 2\,C_2H_4 + Xe \quad (9)$$

$$\rightarrow CoPH_3^+ + 3\,C_2H_4 + Xe \quad (10)$$

$$\rightarrow PEt_3^+ + Co + Xe \quad (11)$$

$$\rightarrow PHEt_2^+ + C_2H_4 + Co + Xe \quad (12)$$

$$\rightarrow PH_2Et^+ + 2\,C_2H_4 + Co + Xe \quad (13)$$

$$\rightarrow Co^+ + PEt_3 + Xe \quad (14)$$

No ligand exchange products were observed (i.e., no ionic products containing Xe were observed in either system). For product channels that contained the cobalt ion, the cross sections displayed little dependence on the Xe reactant pressure; however, the charge-transfer channels, reactions 6, 7, and 11−13, exhibited a modest dependence on pressure. The cross sections shown in Figures 3 and 4 have been extrapolated to zero pressure to eliminate this effect.

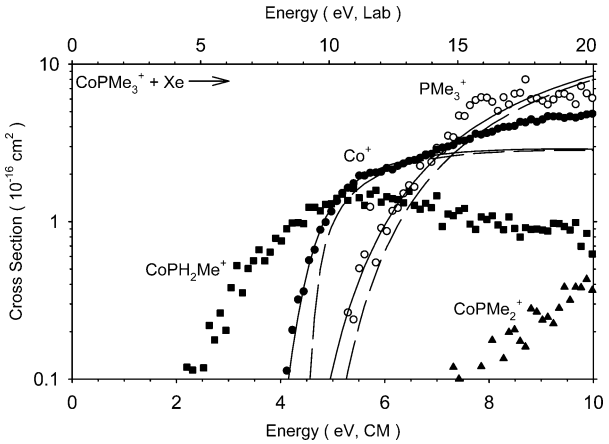

Figure 3. Cross sections for the reaction of $CoPMe_3^+$ with Xe as a function of kinetic energy in the center-of-mass frame (lower *x*-axis) and laboratory frame (upper *x*-axis). Dashed lines are the model for monoenergetic ions having no internal energy, whereas full lines include the distributions of internal and kinetic energies for both reactants.

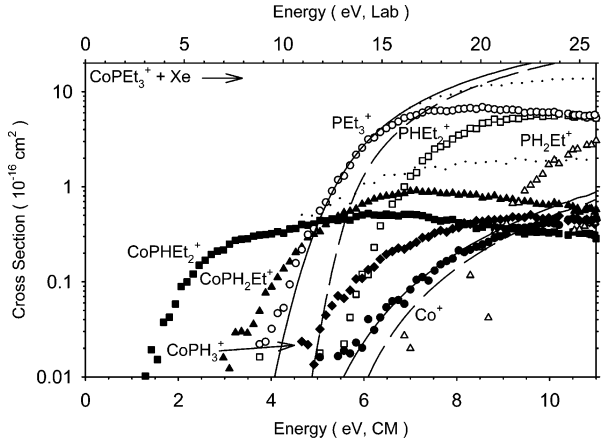

Figure 4. Cross sections for the reaction of $CoPEt_3^+$ with Xe as a function of kinetic energy in the center-of-mass frame (lower *x*-axis) and laboratory frame (upper *x*-axis). The dotted lines show the sums of the cross sections for two sets of products: $PH_x(Et)_{3-x}^+$ ($x = 0-2$) and $CoPH_x(Et)_{3-x}^+$ ($x = 1-3$). Dashed lines are the model for monoenergetic ions having no internal energy, whereas full lines include the distributions of internal and kinetic energies for both reactants.

Data Analysis

Quantum Chemical Calculations. The vibrational frequencies of all neutral and ionic species, as well as the transition states, were required for the TPEPICO and TCID data analysis. For the TPEPICO data analysis, these were used to calculate the internal energy distribution of $Co(CO)_2NOPR_3$ and the dissociating ions, and also for the RRKM statistical rate constant calculations. As discussed below, the four lowest frequencies of the transition states were scaled to fit the experimental TPEPICO dissociation rates, and therefore the accuracy of the individual frequencies was not a real concern. Thus, we used only one level of theory with a sufficiently large basis set. All the calculations were carried out at the DFT level using the B3LYP functional[56] and 6-31++G** basis set for the neutral and dissociating ions. As in the study of $Co(CO)_3NO$,[7] a singlet spin state was calculated for the neutral ground state and a

(56) (a) Becke, A. D. *J. Chem. Phys.* **1992**, *97*, 9173. (b) Lee, C.; Yang, W.; Parr, R. G. *Phys. Rev.* **1988**, *B37*, 785.

Table 1. Vertical and Adiabatic Ionization Energies of PR_3

	PMe_3			PEt_3		
	HF 6-311G**	B3LYP 6-311G**	B3LYP 6-31++G**	HF 6-311G**	B3LYP 6-311G**	B3LYP 6-31++G**
IE_{vert}	7.48	8.52	8.49	7.12	8.14	8.12
IE_{ad}	6.73	7.80	7.77	6.40	7.47	7.45
$IE_{vert} - IE_{ad}$	0.75	0.72	0.73	0.72	0.67	0.67

doublet spin for the nitrosyl containing ionic ground states. For the $CoPR_3^+$ species, the multiplicity of the most stable state was found to be triplet. Because these dissociations proceed with no reverse activation barrier, the transition states do not correspond to a critical point on the potential energy surface. To approximate the vibrational frequencies of the transition states in the PEPICO work, the precursor ion frequencies were used as estimates for the frequencies of the transition states. The Co−L (L = CO, NO) stretch mode was assigned as the critical frequency for the final dissociation step and, thus, deleted. The frequencies used in the data analysis can be viewed in the Supporting Information.

For the analysis of the TCID experiments, the TSs for $CoPR_3^+$ dissociation were modeled as loose associations of the cobalt ion and the neutral phosphine ligand (and cobalt neutral and phosphine ion) because the metal−ligand interactions between the cobalt and the phosphine ligands are largely electrostatic interactions involving ion−dipole and ion-induced dipole forces. This assumption leads to location of the TS at the centrifugal barrier for the products, such that the vibrational frequencies of the TS are those associated with these products. Therefore, no additional calculations of the TS frequencies were required for the CID data analysis.

The dissociation energies obtained from B3LYP/6-31++G** calculations are compared to the experimental values in the data analysis section. All of the above quantum-chemical calculations were carried out with the Gaussian98 program, revision A.11.2.[57]

The adiabatic ionization energies of PMe_3 and PEt_3 are difficult to measure because of the large geometry change upon ionization (the ion is planar). Because the experimentally reported adiabatic IEs do not seem to be well established (see above), the adiabatic and vertical IEs were determined by quantum chemical calculations. The latter were calculated from the energy difference between ground-state neutral PR_3 and the PR_3^+ ion at the neutral's equilibrium geometry. The ionization energies were calculated at various levels of theory (HF/6-311G**, B3LYP/6-311G**, B3LYP/6-31++G**). Results are summarized in Table 1. These results show that the differences between the adiabatic and vertical ionization energies for the two molecules are very similar. Adiabatic ionization energies, calculated with the more accurate CBS-QB3 and CCSD(T)/cc-pVTZ (with B3LYP ZPE) theory, are 7.88 and 7.91 eV, respectively, for PMe_3 and 7.66 and 7.69 eV, respectively, for PEt_3. If the averages (7.89 ± 0.06 and 7.67 ± 0.06 eV) are taken as the adiabatic ionization energies of PMe_3 and PEt_3, respectively, a reasonable accordance with the experiments can be achieved, as discussed below. In the calculations of the ionization energies, the Gaussian03, revision B.05,[58] program was utilized.

TPEPICO Data Analysis. The reaction mechanism for decomposition of the $Co(CO)_2NOPR_3^+$ (R = Me, Et) ions with increasing internal energy involves the sequential loss of two carbonyl and one nitrosyl group in reactions 1−3. The extraction of thermochemical data and bond energies from the experimental results requires an analysis of dissociation rates in terms of the ion internal energy distribution. Detailed descriptions of the TPEPICO data analysis have been discussed in earlier articles.[1,3−7,59−61] Briefly, the ion TOF distributions and the breakdown diagram can be calculated using the following information: the thermal energy distribution of the neutral $Co(CO)_2NOPR_3$, the internal energy distribution of the dissociating ions, the ionization energy, the ion TOF parameters (acceleration electric fields and the acceleration and drift distances), and the transition state vibrational frequencies. RRKM calculations[62,63] were performed to determine the rate constants for the three unimolecular dissociation steps of the $Co(CO)_2NOPR_3^+$ ion. ($k(E)$ plots can be accessed in the Supporting Information.) The following variable parameters were adjusted until the best fit was obtained: the dissociation limits, the four lowest TS vibrational frequencies, and the threshold electron analyzer function. The four lowest vibrational frequencies are ones that are converted from vibrations into overall product rotations. The calculations were carried out minimizing the error between the experimental and calculated TOF distributions and the breakdown diagram. The best fit to both the TOF distributions and the breakdown curves was obtained with the following appearance energies for $CoCONOPMe_3^+$, $CoNOPMe_3^+$, $CoPMe_3^+$, $CoCONOPEt_3^+$, $CoNOPEt_3^+$, and $CoPEt_3^+$ of 8.30, 9.11, 10.80, 8.14, 8.92, and 10.66 eV, respectively. All appearance energy values have uncertainties of 0.05 eV, as discussed below. It is important to point out that, to a first approximation, the determination of each onset is independent of the previous one because in each case we begin from the neutral parent molecule so that the error bars do not increase with each subsequent loss of a ligand. The simulated time-of-flight distributions and breakdown curves are shown as solid curves in Figures 1a−f and 2a,b, respectively.

The uncertainties in the derived parameters were studied by fixing the lowest four transition state frequencies at various values and carrying out the fitting procedure outlined above. This scheme simulates looser and tighter transition states, thereby altering the $k(E)$ rate curves. It was found that changing the lowest four frequencies by ±50% did not affect the simulated breakdown diagram significantly, but the quality of the TOF distributions got significantly worse. This is because the quasi-exponential shape of the asymmetric daughter ion distributions depends on the absolute dissociation rate, whereas the breakdown diagram depends only on the ratios of the rate constants. The optimized appearance energies change by ±0.05 eV, with the altered transition state frequencies given above, which suggests an error bar of ±0.05 eV for these parameters.

(57) Frisch, M. J. et al. *Gaussian 98*, revision A.11.2; Gaussian, Inc.: Pittsburgh, PA, 2001.
(58) Frisch, M. J. et al. *Gaussian 03*, revision B.05; Gaussian, Inc.: Pittsburgh, PA, 2003.
(59) Beyer, T. S.; Swinehart, D. F. *Commun. Assoc. Computing Machinery* **1973**, *16*, 379.
(60) Stein, S. E.; Rabinovitch, B. S. *Chem. Phys. Lett.* **1977**, *49*, 1883.
(61) Baer, T.; Hase, W. L. *Unimolecular Reaction Dynamics: Theory and Experiments*; Oxford University Press: New York, 1996.
(62) (a) Kassel, L. S. *J. Phys. Chem.* **1928**, *32*, 225. (b) Marcus, R. A.; Rice, O. K. *J. Phys. Colloid Chem.* **1951**, *55*, 894. (c) Rice, O. K.; Ramsperger, H. C. *J. Am. Chem. Soc.* **1927**, *49*, 1617.
(63) Gilbert, R. G.; Smith, S. C. *Theory of Unimolecular and Recombination Reactions*; Blackwell Scientific: London, 1990.

Table 2. Comparison of the Experimental and Calculated 0 K Dissociation Energies (eV)

	experimental		calculated[c]	
reaction	L = PMe_3	L = PEt_3	L = PMe_3	L = PEt_3
$Co(CO)_2NOL^+ \rightarrow Co(CO)NOL^+ + CO$[a]	0.94 ± 0.06	0.90 ± 0.06	0.80	0.76
$Co(CO)NOL^+ \rightarrow CoNOL^+ + CO$[a]	0.81 ± 0.07	0.78 ± 0.07	0.84	0.81
$CoNOL^+ \rightarrow CoL^+ + NO$[a]	1.69 ± 0.07	1.74 ± 0.07	1.58	1.59
$CoL^+ \rightarrow Co^+ + L$[b]	2.88 ± 0.11	3.51 ± 0.17	3.16	3.36

[a] From present TPEPICO study. [b] From present TCID study. [c] B3LYP/6-31++G** with ZPE correction.

The derived dissociation energies for reactions 1−3 along with theoretical values generated from B3LYP/6-31++G** calculations are summarized in Table 2. The quantum chemical calculations reproduce the observed trends moderately well.

TCID Results. In the studies detailed here, the kinetic energy dependence of the cross sections for reactions 5, 6, 11, and 14 was analyzed as these product channels yield thermochemistry of direct relevance to $Co(CO)_2NOPR_3$. All of the remaining reaction pathways are either decomposition products of these channels (making it unnecessary to include them in the analysis) or they most likely proceed through tight transition states (making them unlikely to compete effectively with the channels of interest). Further analysis of such remaining channels would necessitate an intensive computational study to find the transition states for these pathways, which is beyond the scope of the present collaborative study.

Previous work from the Armentrout lab has described in detail the modeling of threshold regions for single channel CID processes.[64−66] In the present study, strong competition between the various channels must be explicitly considered to obtain an accurate analysis of the threshold region for the multiple dissociation channels of the $CoPMe_3^+$ and $CoPEt_3^+$ complexes.[67] This is primarily important for an accurate analysis of the higher energy competitive channel threshold. The following competitive modeling equation was used:

$$\sigma_m(E) = \left(\frac{n\sigma_{0,m}}{E}\right)\sum_i g_p \int_0^{E+E_p-E_{0,m}} \left[\frac{k_m(E^*)}{k_{tot}(E^*)}\right]\{1-\exp[-k_{tot}(E^*)\tau]\} (E-\epsilon)^{n-1}\, d(\epsilon) \quad (15)$$

In this equation, $\sigma_{0,m}$ represents an energy-independent scaling factor for the channel m, E is the collision energy, n is an adjustable parameter that represents the efficiency of energy transfer in the collision with Xe,[68] $E_{0,m}$ is the 0 K threshold for the channel m, τ is the experimental time for dissociation ($\sim 5 \times 10^{-4}$ s), ϵ is the energy transferred to internal energy of the complex during the collision of the reactants, and E^* is the total internal energy of the collisionally energized molecule (EM). The summation is over the rovibrational states of the reactant ions having internal energies of E_p and populations of g_p, where $\Sigma g_p = 1$. The Beyer−Swinehart algorithm[59−61] is used to calculate the vibrational energy distribution at 300 K using the frequencies calculated as outlined above. The rate term, $k_m(E^*)$, represents the rate constant for unimolecular dissociation of the reactant complex to channel m, as calculated using RRKM theory.[62,63] It then follows that $k_{tot}(E^*) = \Sigma\, k_m(E^*)$. The frequencies and rotational constants for the complexes and product transition states (TSs) are taken from the theoretical calculations outlined above.

The general form of eq 15 has been found to be suitable for translationally driven reactions[69] and has the ability to reproduce cross sections for numerous reactions of atoms and molecules from diatomic to polyatomic species as well as CID type processes.[10,11,46−49] The model (eq 15) is convoluted with the kinetic energy distribution of the reactants before comparison with the data. The fitting parameters, $\sigma_{0,m}$, $E_{0,m}$, and n, are optimized by performing a nonlinear least-squares analysis compared to the data. The error associated with $E_{0,m}$ includes variations in the parameter n, ±10% scaling of vibrational frequencies, a factor of 2 scaling of the time window available to the ions for dissociation, and the ±0.05 eV (lab) uncertainty in the absolute energy scale for the experiment.

The model of eq 15 includes all sources of energy available to the complex, and therefore the thresholds extracted from this model represent the minimum energy that is needed for the dissociation of the complex, the 0 K value. This conjecture has been tested for a number of systems[10,11,46−49] and has revealed that allowing all the energy in the ionic complex (rotational, vibrational, translational) to couple into the reaction coordinate leads to sensible thermochemistry. To convert 0 K thresholds ($E_{0,m}$) to bond dissociation energies, it is assumed there are no activation barriers to dissociation of reactants to products at 0 K in excess of the bond endothermicities. For ion−molecule reactions,[70] this should hold true for modeling the simple heterolytic and homolytic bond fission reactions studied here.[71]

Ionization Energies of PMe_3 and PEt_3. As discussed in the Introduction, several adiabatic ionization energies of PMe_3 and PEt_3 have been reported in the literature. Because of the large geometry change upon ionization, exact experimental values are difficult to obtain. On the other hand, the vertical ionization energies are readily determined. The analysis of the photoelectron spectra gives an average difference in vertical ionization energies of 0.30 ± 0.05 eV (see above). Ab initio calculations (see the quantum chemical section) were used to demonstrate that this value is correct and the difference in the adiabatic ionization energies can be expected to be similar to this value. Similarly, our CBS-QB3 and CCSD(T)/cc-pVTZ calculations both obtain a difference in the calculated adiabatic ionization energies of 0.22 eV. A recently obtained room-temperature threshold photoelectron spectrum of PEt_3 shows a broad first

(64) Aristov, N.; Armentrout, P. B. *J. Am. Chem. Soc.* **1986**, *108*, 1806.
(65) Rodgers, M. T.; Ervin, K. M.; Armentrout, P. B. *J. Chem. Phys.* **1997**, *106*, 4499.
(66) Armentrout, P. B. *Int. J. Mass Spectrom.* **2000**, *200*, 219.
(67) Rodgers, M. T.; Armentrout, P. B. *J. Chem. Phys.* **1998**, *109*, 1787.
(68) Muntean, F.; Armentrout, P. B. *J. Chem. Phys.* **2001**, *115*, 1213.
(69) Chesnavich, W. J.; Bowers, M. T. *J. Phys. Chem.* **1979**, *83*, 900.
(70) Armentrout, P. B. In *Advances in Gas Phase Ion Chemistry*; Adams, N. G., Babcock, L. M., Eds.; JAI: Greenwich, CT, 1992; Vol. 1, p 83.
(71) Armentrout, P. B.; Simons, J. *J. Am. Chem. Soc.* **1992**, *114*, 8627.

Table 3. Optimized Parameters for CID of $CoPR_3^+$ (R = Me, Et) Complexes with Xe

reactant ion	product ion	σ_0	E_0 (eV)	n
$CoPMe_3^+$	Co^+	5.3 ± 1.1	2.88 ± 0.11	1.2 ± 0.2
	PMe_3^+	107.7 ± 24.1	3.26 ± 0.12	
$CoPEt_3^+$	Co^+	16.9 ± 8.4	3.51 ± 0.17	1.5 ± 0.5
	PEt_3^+		3.13 ± 0.17	

band with a vertical IE of 8.32 ± 0.05 eV.[81] However, it was not possible to obtain a clear onset for the adiabatic IE because the signal descended smoothly into the background noise at about 7.7 eV. Because of the large change in the geometry from tetrahedral to planar, it is probably not possible to obtain an adiabatic IE using photoelectron spectroscopy (PES), a situation that was also encountered in the adiabatic IE of NO_2 that was established to be 9.586 ± 0.002 eV,[72] which is almost 1 eV below the observed onset in the PES.[73] Charge-transfer reactions confirmed the accuracy of this spectroscopic value.[74] When large geometry changes accompany ionization, the use of equilibrium measurements (e.g., charge transfer) are more appropriate because they depend much less on Franck−Condon factors. For the case of PEt_3, such a study was reported by Aue and Bowers[40] some years ago in which they report an adiabatic IE of 7.60 eV, which is in reasonably good agreement with the values calculated here of 7.66 and 7.69 eV. If we add the vertical IE difference of 0.30 eV between ethyl and methyl, we obtain an adiabatic IE of 7.90 eV for the adiabatic IE of PMe_3, which agrees well with the average calculated value of 7.86 ± 0.06 eV.

According to the present TCID experiments, the formation of $Co^+ + PMe_3$ has a threshold lower than that of $PMe_3^+ +$ Co, but the threshold for $Co^+ + PEt_3$ is higher than that of $PEt_3^+ +$ Co. This suggests that the ionization energy of the cobalt atom, $IE(Co) = 7.8810$ eV,[75] falls between the ionization energies of the phosphines, which appears to confirm the adiabatic IEs noted above. However, we can be more quantitative. As shown in Table 3, we measure the CID onset for both the Co^+ and the PR_3^+ channels. In principle, the difference between these onsets should equal the difference in the Co and PR_3 adiabatic IEs. The measured differences between the lower and higher CID thresholds are 0.38 ± 0.03 eV for both reactions, but in opposite directions. (Note that the precision of the difference in threshold energies is higher than that of the absolute values reported in Table 3.) Thus, the CID experiments suggest that the difference between the IEs of PEt_3 and PMe_3 is 0.76 ± 0.04 eV, which is significantly higher than the measured difference in their vertical (and presumably adiabatic) ionization energies of 0.30 ± 0.05 eV and the calculated difference of 0.22 eV. Such a discrepancy is clearly outside the boundaries of our measured or assumed energetics.

This discrepancy in the PR_3 ionization energies can be reconciled by considering the dissocation behavior of the $CoPR_3^+$ complexes more carefully. Heterolytic bond cleavage of $CoPR_3^+$ should yield ground-state $Co^+(^3F, 3d^8) + PR_3(^1A)$, whereas homolytic bond cleavage could lead either to $Co(^4F, 4s^23d^7) + PR_3^+(^2A)$ (adiabatic path) or $Co(^4F, 4s^13d^8) + PR_3^+(^2A)$ (diabatic path), where the latter is an excited-state lying 0.43 eV above the ground-state $Co(^4F, 4s^23d^7)$.[76] The discussion above finds that the difference between the adiabatic ionization energies of the phosphines would be 0.76 ± 0.04 eV if homolytic bond cleavage leads to ground-state $Co(^4F, 4s^23d^7)$ in both systems However, if the formation of the excited-state $Co(^4F, 4s^13d^8)$ is assumed in the dissociation of the $CoPMe_3^+$ complex, the difference in the phosphine IEs is reduced to 0.33 ± 0.04 eV, which is in good accord with the difference of the vertical ionization energies. In fact, we can use the CID threshold energies to calculate adiabatic IEs for PEt_3 that best fit the data. From the $CoPEt_3^+$ CID data and the IE of the cobalt atom, the adiabatic IE of triethylphosphine is 7.50 ± 0.03 eV, somewhat below the 7.61 eV value obtained by Aue and Bowers.[40] From the $CoPMe_3^+$ CID experiment, using the 0.43 eV cobalt excitation energy, we arrive at a trimethylphosphine IE of 7.83 eV, in excellent agreement with the average calculated value of 7.86 ± 0.06 eV. The good agreement between these numbers suggests that the ionization energies determined above are probably correct, and in fact, that competitive CID experiments can be used to determine adiabatic ionization energies when the photoelectron results are ambiguous.

Although the thermochemistry is now self-consistent between the $CoPMe_3^+$ and $CoPEt_3^+$ systems, it remains to be explained why the former dissociates diabatically and the latter adiabatically in the homolytic bond cleavage channel. Such a difference in behavior is possible as illustrated in Figure 5, which shows schematic potential energy surfaces for the dissociation behavior of the two complexes. Full lines show potential energy surfaces in which there are two electrons in the σ bonding space (thereby yielding the ground-state complex), whereas dashed lines indicate surfaces where there is a third electron in the σ space (which necessarily goes into an antibonding orbital such that the bonding interaction is weaker). The repulsive character of the surface evolving from the $Co(s^1d^8) + PR_3^+$ asymptote is correct, as demonstrated by quantum mechanical arguments elsewhere.[71] The key difference between the two systems is the position of the crossing between the surfaces evolving from $Co(s^2d^7) + PR_3^+$ (3 σ electrons) and $Co^+(d^8) + PR_3$ (2 σ electrons). When R = Et, the crossing occurs at a relatively short distance, such that dissociation of $CoPEt_3^+$ can occur adiabatically to the charge-transfer products. In contrast, in the $CoPMe_3^+$ system, formation of $Co + PMe_3^+$ presumably involves electron transfer occurring at much longer range where coupling between the σ^2 and σ^3 surfaces is inefficient, thereby leading to the diabatic behavior observed.

Thermochemical Data

The heats of formation of $Co(CO)_2NOPR_3$ (R = Me, Et) are not listed in any of the major thermochemical compilations.[77−79]

(72) Bryant, G. P.; Jiang, Y.; Martin, M.; Grant, E. R. *J. Chem. Phys.* **1994**, *101*, 7199.
(73) Kimura, K.; Katsumata, S.; Achiba, Y.; Yamazki, T.; Iwata, S. *Handbook of HeI Photoelectron Spectra of Fundamental Organic Molecules*; Japan Scientific Societies Press: Tokyo, Halsted Press: New York, 1980.
(74) Clemmer, D. E.; Armentrout, P. B. *J. Chem. Phys.* **1992**, *97*, 2451.
(75) Page, R. H.; Gudeman, C. S. *J. Opt. Soc. Am. B* **1990**, *7*, 1761.
(76) Sugar, J.; Corliss, C. *J. Phys. Chem. Ref. Data, Suppl. 2* **1985**, *14*, 1.
(77) Cox, J. D.; Pilcher, G. *Thermochemistry of Organic and Organometallic Compounds*; Academic Press: London, 1970.
(78) Rabinovich, I. B.; Nistratov, V. P.; Telnoy, V. I.; Sheiman, M. S. *Thermochemical and Thermodynamic Properties of Organometallic Compounds*; Begell House: New York, 1998.
(79) Linstrom, P. J.; Mallard, W. G. *NIST Chemistry WebBook*; NIST Standard Reference Database Number 69; National Institute of Standards and Technology: Gaithersburg, MD, 2001.
(80) Chase, M. W. *J. Phys. Chem. Ref. Data, Monogr.* **1998**, *9*.
(81) The PEt_3 heat of formation was obtained by a TPEPICO study in which the energy associated with the dissociative photoionization, $P(C_2H_5)_3 + h\nu \rightarrow PH_3^+ + 3\,C_2H_4$, was determined to be 12.48 ± 0.04 eV. Kercher, J. P.; Baer, T. To be submitted for publication.

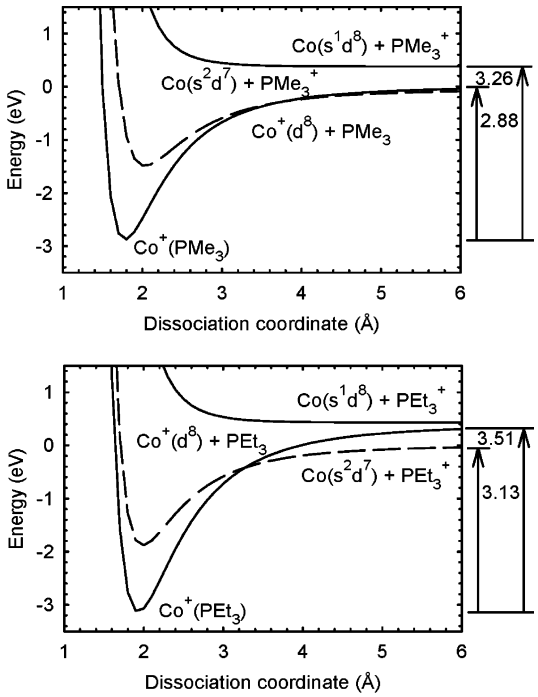

Figure 5. Schematic potential surfaces for the dissociation of $CoPMe_3^+$ and $CoPEt_3^+$. The dissociation energies (eV) are indicated on the right. Long-range potentials are accurately shown, but the positions of the potential wells are approximate.

One approach to obtaining these values is to measure the energy required to dissociatively ionize the molecules to $Co^+ + 2CO + NO + PR_3$. Combining the measured onset with the known product heats of formation permits the determination of the neutral $Co(CO)_2NOPR_3$ heat of formation. The total dissociation energy to the known products is obtained by adding the TPEPICO measured energy for $Co(CO)_2NOPR_3 \rightarrow CoPR_3^+ + 2CO + NO$ to the CID energy for the $CoPR_3^+ \rightarrow Co^+ + PR_3$ reaction. All auxiliary and derived thermochemical data are listed in Table 4 and Figure 6.

Zero Kelvin heats of formation of the Co^+ ion, CO, and NO are taken from the NIST-JANAF thermochemical tables.[80] Zero Kelvin heats of formation of PMe_3[55] and PEt_3 determined by Kercher and Baer[81] are also listed in this table. Combining these data with the Co^+-PMe_3 bond dissociation energy obtained in the TCID experiments, we obtain the $CoPMe_3^+$ 0 K heat of formation, 830 ± 12 kJ/mol (Table 4). For the $CoPEt_3^+$ system, the Co^+-PEt_3 bond dissociation energy of 3.51 ± 0.17 eV suggests that $\Delta_f H_0°(CoPEt_3^+) = 790 \pm 17$ kJ/mol. Alternatively, the $Co-PR_3^+$ bond energies could be combined with the adiabatic ionization energies of the phosphines to obtain the heats of formation of the $CoPR_3^+$ complexes, but the best IE values were clearly not obvious prior to this work.

By combining the $CoPR_3^+$ appearance energies determined in the present TPEPICO experiment with the above derived heats of formation, we obtain the neutral $Co(CO)_2NOPMe_3$ heat of formation of -350 ± 13 kJ·mol^{-1} and the $Co(CO)_2NOPEt_3$ heat of formation of -376 ± 18 kJ·mol^{-1} (Table 4). From the derived heats of formation of the neutral molecules and their adiabatic ionization energies, one can find that the molecular ion $Co(CO)_2NOPMe_3^+$ has a heat of formation of 360 ± 13 kJ·mol^{-1} and the $Co(CO)_2NOPEt_3^+$ heat of formation is 322 ± 18 kJ·mol^{-1}. By combining the neutral molecule heats of formation with the $CoCONOPR_3^+$ appearance energies, the 0 K heats of formation of $CoCONOPMe_3^+$ (565 ± 14 kJ·mol^{-1}) and $CoCONOPEt_3^+$ (523 ± 18 kJ·mol^{-1}) can be obtained. In a similar way, the heats of formation of $CoNOPMe_3^+$ (756 ± 14 kJ·mol^{-1}) and $CoNOPEt_3^+$ (712 ± 19 kJ·mol^{-1}) can also be derived. One can get the $Co-PR_3$ bond energies in each dissociating ionic species if the above derived heats of formation are combined with the heats of formation of the species $Co(CO)_xNO^+$ (x = 2, 1, 0), determined in an earlier study.[7] The derived bond energies are listed in Table 4 and Figure 6.

Using the heat of formation of neutral $Co(CO)_3NO$ published earlier,[7] we obtain reaction enthalpies for the following reactions: $Co(CO)_3NO + PR_3 \rightarrow Co(CO)_2NOPR_3 + CO$, $\Delta_r H$ (0 K) = 18 ± 15 kJ/mol, and $\Delta_r H$ (0 K) = −29 ± 20 kJ/mol for R = Me and Et, respectively. These values are listed in Table 5.

Table 4. Auxiliary and Derived Thermochemical Data (in kJ·mol^{-1})

	D_0 (Co^+–L)	$\Delta_f H_0°$	$\Delta_f H_{298}°$	$H_{298}° - H_0°$
$Co(CO)_2NOPMe_3$		−350 ± 13	−379 ± 13	43.0
$Co(CO)_2NOPEt_3$		−376 ± 18	−423 ± 18	53.6
$Co(CO)_2NOPMe_3^+$	90.7 ± 6.2 (L = CO) 167 ± 16 (L = PMe_3)	360 ± 13	334 ± 13	45.4
$Co(CO)_2NOPEt_3^+$	86.8 ± 6.2 (L = CO) 226 ± 20 (L = PEt_3)	322 ± 18	278 ± 18	56.0
$CoCONOPMe_3^+$	78.2 ± 6.8 (L = CO) 188 ± 16 (L = PMe_3)	565 ± 14	538 ± 14	40.2
$CoCONOPEt_3^+$	75.3 ± 6.8 (L = CO) 250 ± 20 (L = PEt_3)	523 ± 18	479 ± 18	51.3
$CoNOPMe_3^+$	163.1 ± 6.8 (L = NO) 261 ± 16 (L = PMe_3)	756 ± 14	728 ± 14	32.4
$CoNOPEt_3^+$	167.9 ± 6.8 (L = NO) 326 ± 20 (L = PEt_3)	712 ± 19	666 ± 19	43.8
$CoPMe_3^+$	278 ± 11 (L = PMe_3)	830 ± 12	802 ± 13	24.7
$CoPEt_3^+$	339 ± 16 (L = PEt_3)	790 ± 17	745 ± 17	36.0
Co^{+a}		1183.9 ± 1.0		
Co^a		423.5 ± 1.0		4.771
CO^a		−113.81 ± 0.17		
NO^a		89.77 ± 0.17		
PMe_3^b		−76 ± 5	−102 ± 5	20.4
PEt_3^c		−55.3 ± 5	−100 ± 5	31.5

[a] See ref 80. [b] See ref 55. [c] See ref 81.

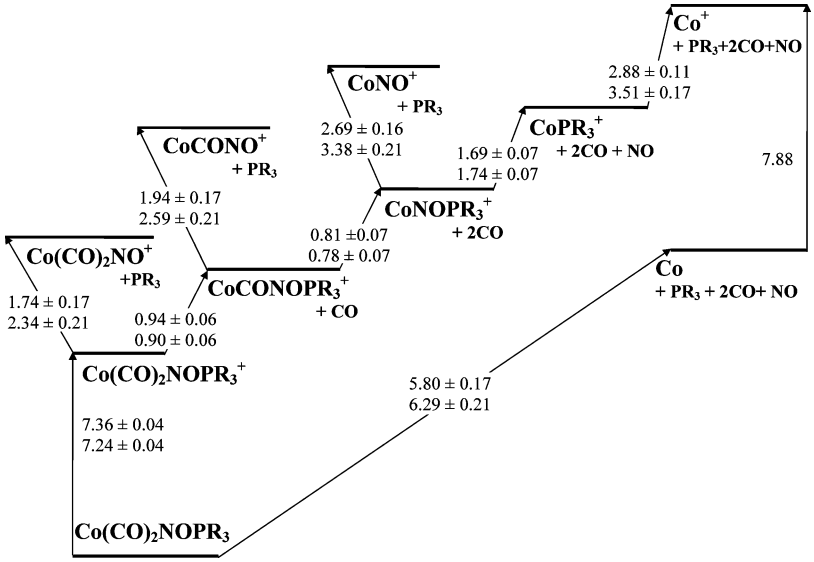

Figure 6. Thermochemistry of the $Co(CO)_2NOPR_3$ (R = Me, Et) systems. Ionization energies and bond energies are indicated in electronvolts with their uncertainties. Data for the R = Me system are always above those for the R = Et system

Table 5. Reaction Enthalpies Derived from the Heats of Formation in Table 4 (in kJ·mol^{-1})

reaction	$\Delta_r H_0°$	$\Delta_r H_{298}°$
$Co(CO)_3NO + PMe_3 \rightarrow Co(CO)_2NOPMe_3 + CO$	18 ± 15	18 ± 16
$Co(CO)_3NO + PEt_3 \rightarrow Co(CO)_2NOPEt_3 + CO$	−29 ± 19	−28 ± 20
$Co(CO)_2NOPMe_3 + PEt_3 \rightarrow Co(CO)_2NOPEt_3 + PMe_3$	−47 ± 23	−46 ± 23

To convert the above thermochemical data to room temperature, one has to calculate $H_{298}° - H_0°$ values for the $Co(CO)_2NOPR_3$ molecules and the various ions. The $H_{298}° - H_0°$ values obtained by using the B3LYP/6-31++G** frequencies are listed in Table 4 with the room-temperature heats of formation of the neutral molecules and ionic species. Using these data along with the $H_{298}° - H_0°$ values of the elements (Co, 4.771 kJ·mol^{-1}; C, 1.051 kJ·mol^{-1}; N_2, 8.670 kJ·mol^{-1}; O_2, 8.683 kJ·mol^{-1}; P, 6.197 kJ·mol^{-1}; H_2, 8.468 kJ·mol^{-1}),[80] we calculated the room temperature heats of formation for $Co(CO)_2NOPR_3$ and its fragments and listed them in Table 4. Throughout these calculations, the Rosenstock (or ion) convention was used, in which the heat capacity of an electron is treated as 0.0 kJ·mol^{-1} at all temperatures.

Conclusion

The TPEPICO and TCID techniques were combined to obtain the gas-phase heats of formation of the $Co(CO)_2NOPR_3$ (R = Me, Et). The 0 K appearance energies of the various fragment ions ($Co(CO)_xNO_yPR_3^+$, $x = 2, 1, 0$; $y = 1, 0$) were determined from the analysis of the TPEPICO experiments. However, the highest photon energy available in the TPEPICO instrument was not enough to observe either bare Co^+ or PR_3^+. The $[Co-PR_3]^+$ bond energies were obtained from the TCID experiments. The data indicate that the dissociation of $CoPMe_3^+$ can yield ground-state $Co^+(^3F, 3d^8) + PMe_3(^1A)$ and excited-state $Co(^4F, 4s^13d^8) + PMe_3^+(^2A)$, where a lower threshold can be assigned to the former reaction. In contrast, $CoPEt_3^+$ dissociates adiabatically to form $Co(^4F, 4s^23d^7) + PEt_3^+(^2A)$ at energies lower than $Co^+(^3F, 3d^8) + PEt_3(^1A)$. On the basis of the TCID experiments, new adiabatic ionization energies of PR_3 (R = Me, Et) are proposed. As a result, it is possible to combine these bond energies with the known heats of formation of Co^+ and PR_3 (R = Me, Et) to derive the 0 K gas-phase heats of formation of the neutral precursors.

The derived $Co-PR_3$ bond energies in the various ionic species show that phosphine ligand is always more strongly bonded to the metal center than the carbonyl and nitrosyl ligands. The triethylphosphine ligand with longer alkyl chains are also harder to remove from the complex than the trimethylphosphine ligand. These findings are in accordance with the higher electron donor capability of the phosphine ligands observed in an earlier photoelectron spectroscopy study.[31]

Combining these heats of formation with the published heat of formation of $Co(CO)_3NO$, we obtain the reaction enthalpy of the carbonyl replacement with the two phosphines. Formation of $Co(CO)_2NOPMe_3$, in gas phase, is less favored thermodynamically than formation of the triethylphosphine derivative.

Acknowledgment. We thank the Hungarian National Science Fund (Országos Tudományos Kutatási Alap) (Grant No. T032489), the U.S. Department of Energy (T.B.), and the National Science Foundation (P.B.A.) for supporting this work. B.S. thankfully acknowledges the generous support of the Magyary Zoltán Fellowship (granted by the Alapítvány a Magyar Felsöoktatásért és Kutatásért). The cooperation between the U.S. and the Hungarian groups was supported by a joint MTA-OTKA-NSF grant.

Note Added after ASAP Publication: In the version published on the Internet June 14, 2005, there were errors in Figure 6. The final version, published June 20, 2005, and the print version are correct.

Supporting Information Available: Calculated (B3LYP/6-31++G**) harmonic vibrational frequencies required for the data analysis (Table 1). Detailed description of the TPEPICO data analysis with the RRKM calculated rate constants of the three dissociation reactions from $Co(CO)_2NOPR_3^+$ (Figure 1) and sample ion internal energy distribution curves of the $Co(CO)_xNOPMe_3^+$ ($x = 2, 1, 0$) species (Figure 2). Full list of authors for refs 57 and 58. This material is available free of charge via the Internet at http://pubs.acs.org.

JA0504744